Journal of Bioscience and Bioengineering
VOL. 127 No. 2, 241–245, 2019

www.elsevier.com/locate/jbiosc

Green synthesis and characterization of iron oxide nanoparticles using *Ficus carica* (common fig) dried fruit extract

Derya Aksu Demirezen,[1,2,*] Yalçın Şevki Yıldız,[3] Şeyda Yılmaz,[1,2] and Dilek Demirezen Yılmaz[2,4]

Graduate School of Natural and Applied Sciences, Erciyes University, Talas 38280, Kayseri, Turkey,[1] NanoBiotech, Erciyes Teknopark, Talas 38280, Kayseri, Turkey,[2] Environmental Engineering Department, Faculty of Engineering, Erciyes University, Talas 38280, Kayseri, Turkey,[3] and Biology Department, Faculty of Sciences, Erciyes University, Talas 38280, Kayseri, Turkey[4]

Received 6 March 2018; accepted 27 July 2018
Available online 20 October 2018

Ficus carica **(common fig) dried fruit extract was used to synthesize iron oxide nanoparticles in this study. Biomaterials in the common fig dried fruit extract synthesized the iron nanoparticles by reducing the iron precursor salt and then acted as capping and stabilizing agents. The nanoparticles were produced smaller than 20 nm diameters and oxidized due to the high phenolic compound content in the common fig dried fruit extract. Nanoparticles were characterized by energy dispersive X-ray spectroscopy (EDX), transmission electron microscopy (TEM), UV-visible spectroscopy, X-ray diffraction (XRD), Fourier transform infrared spectroscopy (FTIR), dynamic light scattering (DLS). First, color change and pH reduction occurred immediately due to the iron nanoparticle synthesis. TEM images showed that the nanoparticles were at 9 ± 4 nm diameters and the metallic core-oxide shell form. The nanoparticles were in spherical shapes with a monodisperse distribution. EDX, XRD and FTIR analysis signals showed the iron oxyhydroxide/oxide formation. Absorption peaks were detected at 205 nm and 291 nm due to the iron metallic core hydrolysis products. The intensity-average diameter of nanoparticles was calculated at 475 nm diameter by DLS analysis. Colloid stability was determined as moderate at 20.7 mV.**

[**Key words:** Iron oxide nanoparticle; Biomedical application; Green synthesis; Bioreduction; Plant extract; *Ficus carica*]

Iron oxides are chemical structures comprising iron and oxygen. There are several forms of iron oxide such as iron (II) oxide (wüstite), iron (II, III) oxide (magnetite), iron (III) oxide (hematite/maghemite). Iron (III) oxide or ferric oxide is one of the three main of iron oxides. It is paramagnetic, has a reddish-brown color, and often called as rust (1).

Nanoparticles have become widespread in many areas by their advanced features. They are preferred due to the high surface area, low toxicity, and easy separation properties. Iron oxide nanoparticles such as maghemite or magnetite that are smaller than 20 nm have unique properties (2). They are used in biomedical applications for diagnostic magnetic resonance imaging (MRI), drug delivery to a cell or tissue, and cell biology research to separate and purify cell populations (3). The toxicity of iron oxide nanoparticles is changing due to the concentration and exposure time. They are cleared from the body at lower concentrations (<10 mg/mL) and exposure time (<72 h). They may cause cellular stress (oxidative) and alter the response such as DNA, gene expression at high doses. More studies still are needed in this direction (4).

Iron oxide nanoparticles are produced in magnetite, maghemite and hematite forms by physical, chemical and biological methods (5). Plants are used for the iron oxide nanoparticles synthesis among the biological methods. Different plant parts are used such as root, seed, fruit, and leaf. Phytochemicals play an important role in the nanoparticle production as the green approach to nanotechnology.

Iron oxide nanoparticles have been produced by several plant extracts such as green tea leaf, carob leaf, and pomegranate leaf (6). Biomaterials are the phenolic and nitrogen compounds, vitamins, sugar, terpenoids, and proteins that are found in the extract. They act as reducing, capping and stabilizing agents. There are factors affecting the nanoparticle size, morphology and distribution. The most important ones are the biomaterial content and drying temperature. The drying temperature is important for preserving the biomaterials while the solvent is essential to extracting them (7).

Ficus carica (common fig) dried fruit contains vitamins, minerals, carbohydrates, sugars, organic acids, and phenolic compounds. The dried fig is the excellent source of fiber and polyphenols (8).

MATERIALS AND METHODS

Materials and procedures *F. carica* (common fig) dried fruit was purchased from a local shop in Kayseri, Turkey. Ferric chloride hexahydrate ($FeCl_3 \cdot 6H_2O$) was purchased from Merck KGaA, Germany. Double distilled water was used.

The chemical extraction yield depends on the solvent, plant drying, treatment, time, temperature, and the plant to the solvent ratio (9). Dried fruit was chopped into fine particles with a plastic knife, 10 g weighed and put into 150 mL double distilled water. The solution was heated at 100°C in a closed beaker for 1 h and then filtered with Whatman No. 1 paper.

$FeCl_3 \cdot 6H_2O$ (3.8 g) was dissolved in 100 mL of distilled water to prepare a 0.14 M ferric chloride solution. It was stirred for 15 min.

* Corresponding author at: Graduate School of Natural and Applied Sciences, Erciyes University, Talas, 38280, Kayseri, Turkey. Tel.: +90 5322758315; fax: +90 3525030301.

E-mail addresses: dademirezen@gmail.com (D. Aksu Demirezen), yyildiz@erciyes.edu.tr (Y.Ş. Yıldız), seyda.yilmaz100@gmail.com (Ş. Yılmaz), demirezen.dilek@gmail.com (D. Demirezen Yılmaz).

1389-1723/$ – see front matter
https://doi.org/10.1016/j.jbiosc.2018.07.024

Extract and ferric chloride solutions were mixed at a volume of 1:1 ratio and then stirred by a magnetic stirrer for 2 h. A sudden color change occurred which is the indicator of nanoparticle production. Nanoparticle solution was centrifuged at 4000 rpm for 40 min. The residue dried at 60°C in a laboratory oven for 24 h.

Characterization of iron nanoparticles Transmission electron microscopy (TEM) analysis was used to observe the iron oxide nanoparticles size, morphology, and distribution. Dynamic light scattering (DLS) analysis was used for hydrodynamic diameter calculation. Zeta potential (ZP) analysis was used to determine colloid stability. Elemental content of nanoparticle was analyzed by EDX spectrum. X-ray diffraction (XRD) analysis was used to determine the iron oxide forms. Fourier transform infrared spectroscopy (FTIR) analysis was used to identify the oxide forms and the biomaterials on the surface of the nanoparticle. UV-visible spectroscopy was used to get the absorption spectrum of iron hydrolysis products. pH was measured.

RESULTS AND DISCUSSION

Iron oxide nanoparticle synthesis The color changed from golden (Fig. 1a) to the brown (Fig. 1b) suddenly. This was the indicator of ferric ion reduction. Iron nanoparticle formation is shown in Eq. 1. This is the mechanism of iron nanoparticles synthesis by polyphenols. *Ar* and *n* stand for the aromatic ring and the oxidized group number, respectively (10).

$$nFe^{3+} + 3(Ar\text{-}OH)_n \rightarrow nFe^0 + 3\ (\text{aromatic ring} = O)_n + 3nH^+\ (aq) \quad (1)$$

Iron nanoparticles were formed in core–shell form due to the metallic core oxidation. There are several phases in iron oxide formation and color differs for each form. For example, magnetite has a black color, maghemite has light brown colors, and hematite has red colors (11). The extract pH reduced to 2.21 from 5.29 immediately after iron nanoparticle production. This pH drop observed in several studies such as with mango from 5.12 to 2.16, with clove from 4.22 to 1.88, with green tea from 5.37 to 2.65, and with carom seeds from 5.76 to 3.89 (12). The metal core oxidation is occurred by water. Ferric ions are generated by oxidation which is shown in Eqs. 2 and 3. Ferric hydroxide precipitates on the surface of the iron metallic core and is dehydrated to oxyhydroxide as shown in the Eqs. 4 and 5. Ferric oxyhydroxide is converted to iron oxide product as shown in Eq. 6 (13).

$$2Fe^0\ (s) + 2H_2O\ (l) \rightarrow 2Fe^{2+} + H_2\ (g) + 2OH^-\ (aq) \quad (2)$$

$$2Fe^{2+} + 2H_2O\ (l) \rightarrow 2Fe^{3+} + H_2\ (g) + 2OH^-\ (aq) \quad (3)$$

$$2Fe^{3+} + 3OH^- \rightarrow Fe\ (OH)_3 \downarrow \quad (4)$$

$$Fe(OH)_3 \rightarrow FeOOH \downarrow + H_2O \quad (5)$$

$$FeOOH \rightarrow Fe_2O_3 + H_2O \quad (6)$$

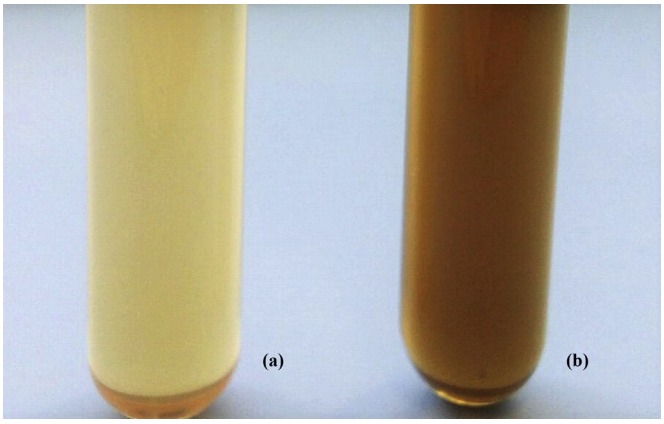

FIG. 1. (a) Common fig dried fruit extract. (b) Iron nanoparticles solution.

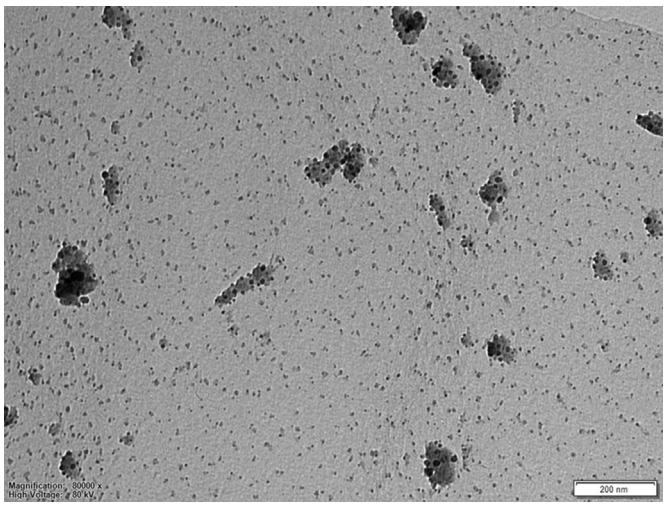

FIG. 2. TEM image showing distribution of iron nanoparticles.

Iron oxide nanoparticle characterization Size, shape, and distribution of the nanoparticles were analyzed by TEM. Nanoparticles were in a monodisperse distribution (Fig. 2) and the polydispersity index was calculated at 0.18. Agglomerations were detected due to the inadequate capping agents that cause the hydrophobic surface (14). Nanoparticles were determined in the spherical shape (Fig. 3) at 9 ± 4 nm average diameter (Fig. 4). Dark center with the gray edge that is attributed to the metallic core and the oxide layer was seen in the TEM images (15).

The atomic percentages of elements were at 71.35 % oxygen, 8.46 % iron, 19.19 % chlorine, and 1.01 % K due to the EDX analysis. The high percentage of oxygen showed that the nanoparticles are at iron oxide form. K content is related to the plant constituent (16).

The X-ray diffraction (XRD) analysis of fresh nanoparticles is shown in Fig. 5 at the 2θ. The distinctive peaks appeared at 14°, 27°, 49°, and 63°. Iron oxide peak due to the maghemite was detected at 63°. Iron oxyhydroxide peaks due to the lepidocrocite were detected at 14°, 27°, and 49° (17).

The intensity-average diameter of nanoparticles was calculated at 475 nm by DLS analysis. Hydrodynamic size distribution is shown in Fig. 6. It is the size of the core along with the capping materials around it (18).

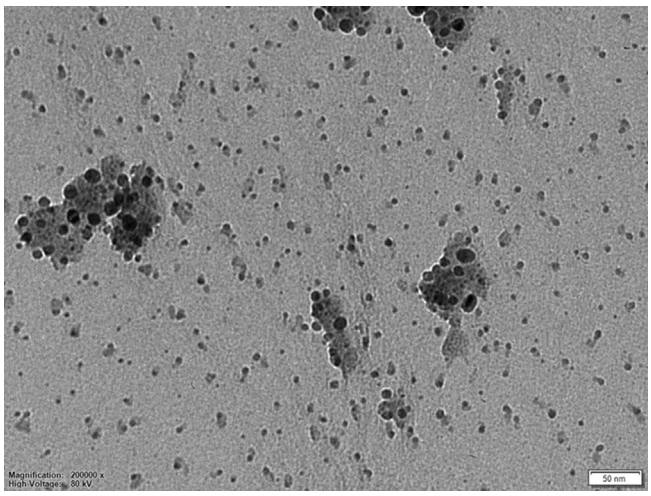

FIG. 3. TEM image showing shape and core–shell of iron nanoparticles.

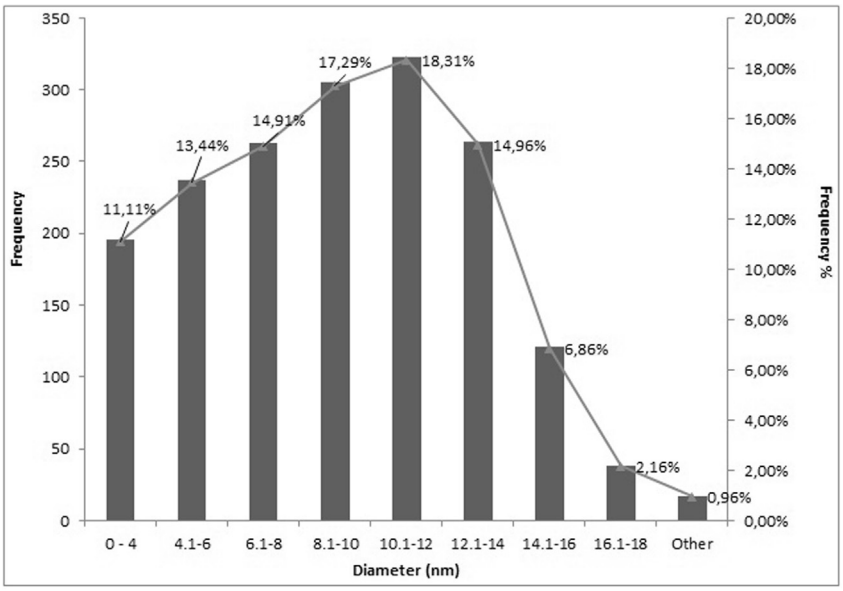

FIG. 4. TEM image showing size distribution.

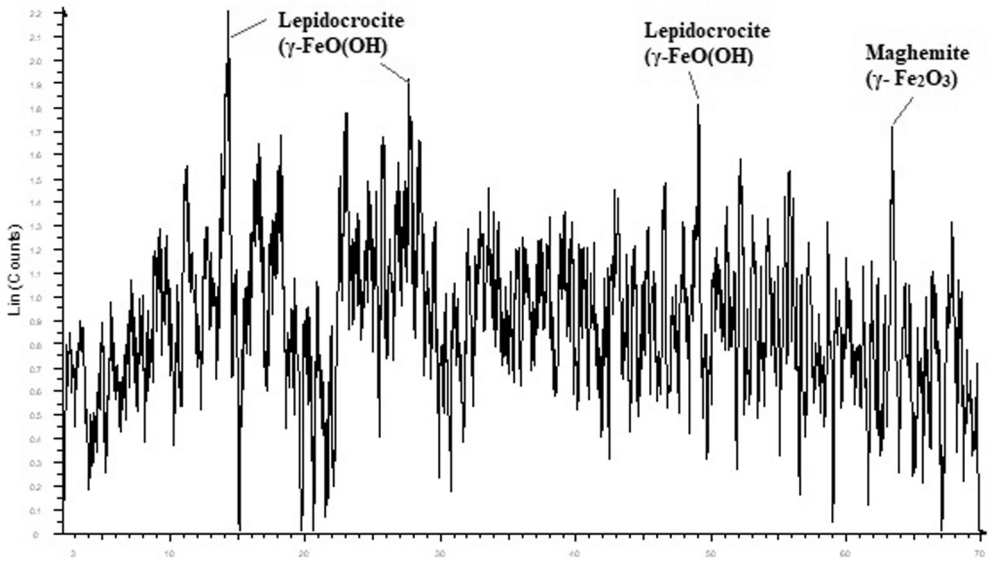

FIG. 5. XRD image showing the iron oxide forms.

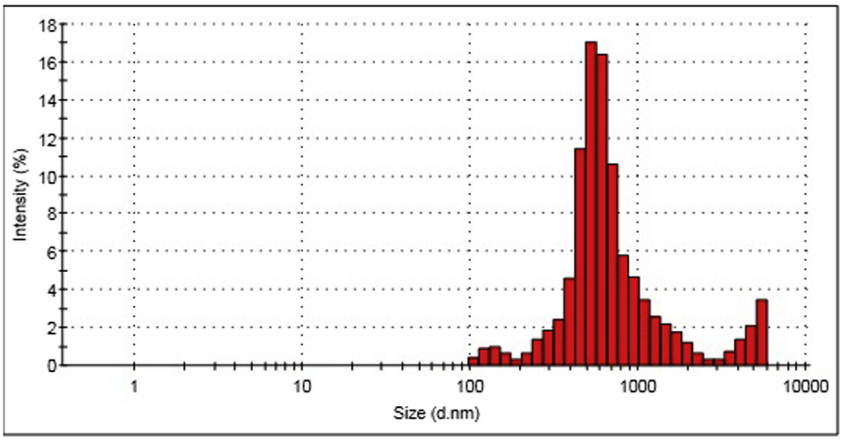

FIG. 6. DLS image showing hydrodynamic diameter.

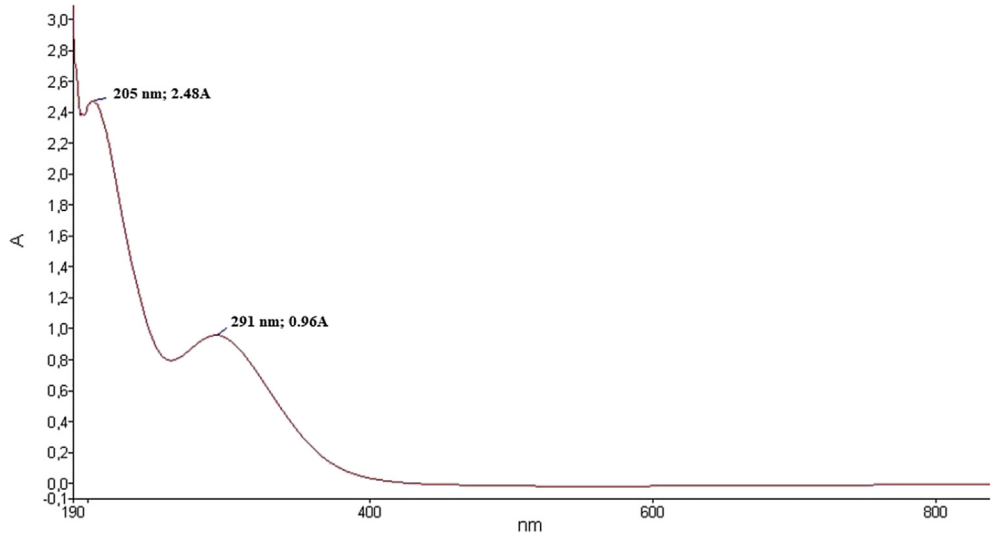

FIG. 7. UV-visible spectra image showing absorption peaks.

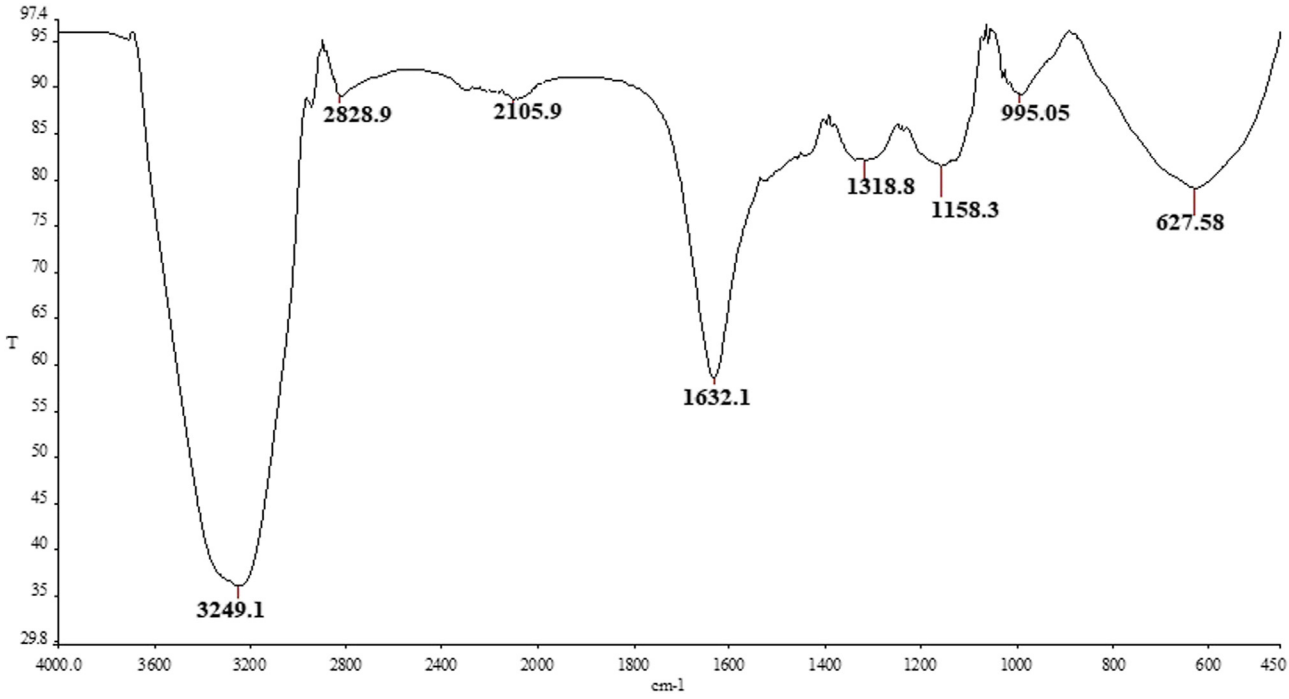

FIG. 8. FTIR spectrum image of iron nanoparticles.

Zeta potential was measured at 20.7 mV. It shows that the aqueous stability is moderate and establishes the good interactions of biomaterials (19).

UV absorption peaks shown in Fig. 7 were detected at 205 and 291 nm. These were occurred due to the ferric ion hydrolysis products and precipitated on the surface of the nanoparticle (20).

FTIR analysis shown in Fig. 8 was used to identify the iron oxide forms. IR band at the 3249.1 belongs to the OH group between 2500 and 3800 cm^{-1} (21). Fe–O vibrations at the lower wavenumber bands belong to the iron oxide nanoparticles. Magnetite band is observed at 400 and 570 cm^{-1}. Maghemite band is observed between 620 and 660 cm^{-1}. Hematite band is observed at 352, 470, and 540 cm^{-1} (22). Therefore, Fe–O stretches at the 627.58 cm^{-1} belongs to the maghemite nanoparticles.

The other bands in FTIR spectrum occurred due to the *F. carica* (common fig) dried fruit extract biomaterials. These are the hydrophilic groups such as hydroxyl and carbonyl. These groups provide stable nanoparticles by increasing the interactions with water molecules (23). The O–H stretch of the carboxylic acid signal appeared at 2829 cm^{-1}. Weak stretching C≡C alkyne was seen at 2105.9 cm^{-1}. C=O carbonyl stretching vibration of alkene was seen at 1632.1 cm^{-1}. Strong C–O acyl derived from carboxylic acid appeared at 1318.8 cm^{-1}. The alkoxy C–O bond signal appeared at the 1158.3 cm^{-1}. C–H alkene bending appeared at 995.05 cm^{-1}.

Conclusion Iron oxide nanoparticles were produced by the biological materials found in the *F. carica* (common fig) dried fruit extract. Nanoparticles were synthesized at maghemite (γ-Fe_2O_3) form and were at the average diameter of 9 ± 4 nm in spherical

shapes. Nanoparticle solution was at moderate stability and well dispersion. As a result, the nanoparticles are suitable at the usage in living organisms in biomedical applications due to the lowered side effects instead of chemical production nanoparticles. The green production of well-stabilized nanoparticles is a promising development because of the lack of toxic chemicals usage and excessive energy consumption.

ACKNOWLEDGMENTS

The authors declare no conflict of interest.

References

1. **Bernal, J. D., Dasgubta, D. R., and Mackay, A. L.:** The oxides and hydroxides of iron and their structural inter-relationships, Clay Miner., **4**, 15–30 (1959).
2. **Ramimoghadam, D., Bagheri, S., and Abd Hamid, S. B.:** Progress in electrochemical synthesis of magnetic iron oxide nanoparticles, J. Magn. Magn. Mater., **368**, 207–229 (2014).
3. **Tartaj, P., Morales, M. P., González-Carreño, T., Veintemillas-Verdaguer, S., and Serna, C. J.:** Advances in magnetic nanoparticles for biotechnology applications, J. Magn. Magn. Mater., **290–291**, 28–34 (2005).
4. **Patil, R. M., Thorat, N. D., Shete, P. B., Bedge, P. A., Gavde, S., Joshi, M. G., Tofail, S. A. M., and Bohara, R. A.:** Comprehensive cytotoxicity studies of superparamagnetic iron oxide nanoparticles, Biochem. Biophys. Rep., **13**, 63–72 (2018).
5. **Attarad, A., Hira, Z., Muhammad, Z., İhsan, H. U., Rehman, P. A., Joham, A. S., and Altaf, H.:** Synthesis, characterization, applications, and challenges of iron oxide nanoparticles, Nanotechnol. Sci. Appl., **9**, 49–67 (2016).
6. **Saif, S., Tahir, A., and Chen, Y.:** Green synthesis of iron nanoparticles and their environmental applications and implications, Nanomaterials (Basel), **6**, 209 (2016).
7. **Mohamad, N. A. N., Arham, N. A., Jai, J., and Hadi, A.:** Plant extract as reducing agent in synthesis of metallic nanoparticles: a review, Adv. Mater. Res., **832**, 350–355 (2013).
8. **Mawa, S., Husain, K., and Jantan, I.:** *Ficus carica* L. (Moraceae): phytochemistry, traditional uses and biological activities, Evid. Based Complement. Alternat. Med., **2013**, 974256 (2013).
9. **Dai, J. and Mumper, R. J.:** Plant phenolics: extraction, analysis and their antioxidant and anticancer properties, Molecules, **15**, 7313–7352 (2010).
10. **Borja, J. Q., Ngo, M. A. S., Saranglao, C. C., Tiongco, R. P. M., Roque, E. C., and Dugos, N. P.:** Synthesis of green zero-valent iron using polyphenols from dried green tea extract, J. Eng. Sci. Technol., **10**, 22–31 (2015).
11. **Katikaneani, P., Vaddepally, A. K., Tippana, N. R., Banavath, R., and Kommu, S.:** Phase transformation of iron oxide nanoparticles from hematite to maghemite in presence of polyethylene glycol: application as corrosion resistant nanoparticle paints, J. Nanosci., **2016**, 1328463 (2016).
12. **Pattanayak, M. and Nayak, P. L.:** Ecofriendly green synthesis of iron nanoparticles from various plant and spices extract, J. Plant Anim. Environ. Sci., **3**, 68–78 (2013).
13. **Mu, Y., Jia, F., Ai, Z., and Zhang, L.:** Iron oxide shell mediated environmental remediation properties of nano zero-valent iron, Environ. Sci. Nano, **4**, 27–45 (2017).
14. **Wu, W., He, Q., and Jiang, C.:** Magnetic iron oxide nanoparticles: synthesis and surface functionalization strategies, Nanoscale Res. Lett., **3**, 397–415 (2008).
15. **Martin, J. E., Herzing, A. A., Yan, W., Li, X., Koel, B. E., Kiely, C. J., and Zhang, W.:** Determination of the oxide layer thickness in core-shell zerovalent iron nanoparticles, Langmuir, **24**, 4329–4334 (2008).
16. **Solomon, A., Golubowicz, S., Yablowicz, Z., Grossman, S., Bergman, M., Gottlieb, H. E., Altman, A., Kerem, Z., and Flaishman, M. A.:** Antioxidant activities and anthocyanin content of fresh fruits of common fig (*Ficus carica* L.), J. Agric. Food Chem., **54**, 7717–7723 (2006).
17. **Liu, A., Liu, J., Pan, B., and Zhang, W.:** Formation of lepidocrocite (γ-FeOOH) from oxidation of nanoscale zero-valent iron (nZVI) in oxygenated water, RSC Adv., **4**, 57377–57382 (2014).
18. **Lim, J., Yeap, S. P., Che, H. X., and Low, S. C.:** Characterization of magnetic nanoparticle by dynamic light scattering, Nanoscale Res. Lett., **8**, 381 (2013).
19. **Bhattacharjee, S.:** DLS and zeta potential – what they are and what they are not? J. Control. Release, **235**, 337–351 (2016).
20. **Stefánsson, A.:** Iron (III) hydrolysis and solubility at 25°C, Environ. Sci. Technol., **41**, 6117–6123 (2007).
21. **Betancur, A., Correa, M., Perez, F. R., and Barrero, C. A.:** Quantitative approach in iron oxides and oxyhydroxides by vibrational analysis, Opt. Pura Apl., **45**, 269–275 (2012).
22. **Namduri, H. and Nasrazadani, S.:** Quantitative analysis of iron oxides using fourier transform infrared spectrophotometry, Corros. Sci., **50**, 2493–2497 (2008).
23. **Ebrahiminezhad, A., Zare-Hoseinabadi, A., Berenjian, A., and Ghasemi, Y.:** Green synthesis and characterization of zero-valent iron nanoparticles using stinging nettle (*Urtica dioica*) leaf extract, Green Process. Synth., **6**, 469–475 (2017).